Biochimica et Biophysica Acta 1807 (2011) 119–129

Contents lists available at ScienceDirect

Biochimica et Biophysica Acta

journal homepage: www.elsevier.com/locate/bbabio

Probing the quinone binding site of Photosystem II from *Thermosynechococcus elongatus* containing either PsbA1 or PsbA3 as the D1 protein through the binding characteristics of herbicides

Alain Boussac [a,*], Miwa Sugiura [b,*], Fabrice Rappaport [c,*]

[a] *iBiTec-S, CNRS URA 2096, CEA Saclay, 91191 Gif-sur-Yvette, France*
[b] *Cell-Free Science and Technology Research Center, Ehime University, Bunkyo-cho, Matsuyama Ehime, 790-8577 and PRESTO, JST, Honcho, Kawaguchi, Saitama,332-0012, Japan*
[c] *Institut de Biologie Physico-Chimique, UMR 7141 CNRS and Université Pierre et Marie Curie, 13 rue Pierre et Marie Curie, 75005 Paris, France*

ARTICLE INFO

Article history:
Received 15 July 2010
Received in revised form 23 September 2010
Accepted 4 October 2010
Available online 16 October 2010

Keywords:
Photosystem II
D1 protein
PsbA protein
Herbicide
EPR
Absorption change

ABSTRACT

The main cofactors involved in Photosystem II (PSII) oxygen evolution activity are borne by two proteins, D1 (PsbA) and D2 (PsbD). In *Thermosynechococcus elongatus*, a thermophilic cyanobacterium, the D1 protein is predominantly encoded by either the *psbA$_1$* or the *psbA$_3$* gene, the expression of which depends on the environmental conditions. In this work, the Q_B site properties in PsbA1-PSII and PsbA3-PSII were probed through the binding properties of DCMU, a urea-type herbicide, and bromoxynil, a phenolic-type herbicide. This was done by using helium temperature EPR spectroscopy and by monitoring the time-resolved changes of the redox state of Q_A by absorption spectroscopy in PSII purified from a His_6-tagged WT strain expressing PsbA1 or from a His_6-tagged strain in which both the *psbA$_1$* and *psbA$_2$* genes have been deleted and which therefore only express PsbA3. It is shown that, in both PsbA1-PSII and PsbA3-PSII, bromoxynil does not bind to PSII when Q_B is in its semiquinone state which indicates a much lower affinity for PSII when Q_A is in its semiquinone state than when it is in its oxidized state. This is consistent with the midpoint potential of $Q_A^{\bullet-}/Q_A$ being more negative in the presence of bromoxynil than in its absence [Krieger-Liszkay and Rutherford, Biochemistry 37 (1998) 17339–17344]. The addition in the dark of DCMU, but not that of bromoxynil, to PSII with a secondary electron acceptor in the $Q_B^{\bullet-}$ state induces the oxidation of the non-heme iron in a fraction of PsbA3-PSII but not in PsbA1-PSII. These results are explained as follows: *i*) bromoxynil has a lower affinity for PSII with the non-heme iron oxidized than DCMU therefore, *ii*) the midpoint potential of the Fe^{II}/Fe^{III} couple is lower with DCMU bound than with bromoxynil bound in PsbA3-PSII; and *iii*) the midpoint potential of the Fe^{II}/Fe^{III} couple is higher in PsbA1-PSII than in PsbA3-PSII. The observation of DCMU-induced oxidation of the non-heme iron leads us to propose that Q_2, an electron acceptor identified by Joliot and Joliot [FEBS Lett. 134 (1981) 155–158], is the non-heme iron.

1. Introduction

Light-driven water oxidation by the Photosystem II (PSII) enzyme is responsible for the production of O_2 on Earth and is at the origin of the synthesis of most of the biomass. Refined three dimensional X-ray structures from 3.5 Å to 2.9 Å resolution have been obtained using PSII isolated from the thermophilic cyanobacterium *Thermosynechococcus elongatus* [1–3]. PSII is made up of 17 membrane protein subunits, 3 extrinsic proteins, 35 chlorophyll molecules, 2 pheophytin molecules, 2 hemes, 1 non-heme iron, 2 (+1) quinones, 4 Mn ions, 1 Ca^{2+} [1–3] and at least 1 Cl^- [3–5], 12 carotenoid molecules and 25 lipids [3].

Absorption of a photon by a chlorophyll molecule is followed by the transfer of the exciton to the photochemical trap and the consecutive formation of a radical pair in which the pheophytin molecule, $Pheo_{D1}$, is reduced and the chlorophyll molecule, Chl_{D1}, is oxidized [6–8]. The positive charge is then stabilized on P_{680}, a weakly coupled chlorophyll dimer (see *e.g.* [9–12] for energetic considerations). $P_{680}^{\bullet+}$ oxidizes a tyrosine residue of the D1 polypeptide, Tyr_Z, which in turn oxidizes the Mn_4Ca-cluster. The pheophytin anion ($Pheo_{D1}^{\bullet-}$) transfers the electron to the primary quinone electron acceptor, Q_A, which in turn reduces a second quinone, Q_B. Q_A is tightly bound and acts as a one-electron carrier whereas Q_B acts as a two-electron and two-proton acceptor with a stable semiquinone intermediate, $Q_B^{\bullet-}$. While the $Q_B^{\bullet-}$ semiquinone

Abbreviations: PSII, Photosystem II; Chl, chlorophyll; PPBQ, phenyl-*p*-benzoquinone; MES, 2-(N-morpholino) ethanesulfonic acid; P_{680}, primary electron donor; Q_A, primary quinone acceptor; Q_B, secondary quinone acceptor; TL, thermoluminescence; 43H, *T. elongatus* strain with a His-tag on the C terminus of CP43; WT*, *T. elongatus* strain with a His-tag on the C terminus of CP43 and in which the *psbA$_1$* and *psbA$_2$* genes are deleted; EPR, Electron Paramagnetic Resonance; DCMU, 3-(3,4-dichlorophenyl)-1, 1-dimethylurea; PQ, plastoquinone 9; D2-Y160F, site-directed mutant without the tyrosine Tyr_D

* Corresponding authors.
E-mail addresses: alain.boussac@cea.fr (A. Boussac), miwa.sugiura@ehime-u.ac.jp (M. Sugiura), fabrice.rappaport@ibpc.fr (F. Rappaport).

0005-2728/$ – see front matter © 2010 Elsevier B.V. All rights reserved.
doi:10.1016/j.bbabio.2010.10.004

state is tightly bound, its quinone and quinol forms are exchangeable with the quinone pool in the thylakoid membrane [13–17].

The Mn_4Ca-cluster, a device accumulating the four oxidizing equivalents required to split water into dioxygen, is the active site for water oxidation. During the enzyme cycle, the oxidizing side of PSII goes through five sequential redox states, denoted S_n where n varies from 0 to 4 upon the absorption of 4 photons [18,19]. Upon formation of the S_4 state two molecules of water are rapidly oxidized, O_2 is released and the S_0-state is regenerated.

The main cofactors involved in the function of PSII are borne by D1 and D2 proteins. There are three *psbA* genes encoding the D1 protein in the *T. elongatus* genome [20]. The comparison of the amino-acid sequence deduced from the $psbA_3$ gene to that deduced from the $psbA_1$ and $psbA_2$ genes points a difference of 21 and 31 residues, respectively. In *T. elongatus*, the acclimation to high light intensities induces the expression of the $psbA_3$ gene to the detriment of the $psbA_1$ gene [21,22]. We have proposed that this regulation at the transcription level is not a mere adjustment of the protein synthesis but rather an acclimation at the functional level whereby the functional properties of PSII are adjusted to cope with the increased photon flux [23].

Amongst the 21 amino acids which differ between PsbA1 and PsbA3 like D1-S270A, D1-S153A and D1-Q130E (see [23] for a discussion), the residue at position 130 has caught much attention. It is a Gln in PsbA1 and a Glu in PsbA3. The Gln to Glu exchange is expected to stabilize the $Pheo_{D1}^{\bullet-}$ anion radical [24–27] and it has been shown that, accordingly, the midpoint potential of $Pheo_{D1}$ is increased by 17 mV from −522 mV in PsbA1-PSII [23] to −505 mV in PsbA3-PSII [12]. This increase is about half that found in the single D1-Q130E site-directed mutant in *Synechocystis* PCC 6803 [24–27]. This led us to propose that the effects of the D1-Q130E substitution could be, at least partly, compensated for by some of the additional amino-acid changes associated with the PsbA3 for PsbA1 substitution [23]. The electron transfer rate between $P_{680}^{\bullet+}$ and Y_Z was also found faster in PsbA3 than in PsbA1 which suggests a change in either the midpoint potential of either Y_Z or $P_{680}/P_{680}^{\bullet+}$ couple (and hence that of $P_{680}^{*}/P_{680}^{\bullet+}$) or in the reorganization energy or less likely in the distance between P_{680} and Y_Z when shifting from PsbA1 to PsbA3. To assess the possible differences of the Q_A/Q_B binding sites we have compared here the binding properties of herbicides to the PsbA1-PSII and PsbA3-PSII.

Two different classes of compounds are known to inhibit the reoxidation of $Q_A^{\bullet-}$ by Q_B: urea derivative herbicides such as DCMU and phenolic herbicides such as bromoxynil. These two types of compounds have been shown to have opposite consequences on the midpoint potential of the $Q_A^{\bullet-}/Q_A$ couple [28,29]. In plant PSII, DCMU increases the midpoint potential of $Q_A^{\bullet-}/Q_A$ (making it less negative), conversely, bromoxynil decreases the midpoint potential of $Q_A^{\bullet-}/Q_A$ (making it more negative) [28,29]. The binding of bromoxynil induces a decrease of the free energy gap between the $^1[P_{680}^{\bullet+}Q_A^{\bullet-}]$ and the $^1[P_{680}^{\bullet+}Pheo_{D1}^{\bullet-}]$ radical pairs which favors the formation of the $^1[P_{680}^{\bullet+}Pheo_{D1}^{\bullet-}]$ by reverse electron transfer and therefore the formation of the $^3[P_{680}^{\bullet+}Pheo_{D1}^{\bullet-}]$ state and then $^3P_{680}$. Since $^3P_{680}$ can react with oxygen, forming singlet oxygen, a species likely responsible for photodamage, it has been proposed that, in plant PSII, phenolic herbicides increase the sensitivity of PSII to light, while DCMU protects against photodamage [28,29].

In *T. elongatus*, the relative effects of DCMU and bromoxynil on the midpoint potential of the $Q_A^{\bullet-}/Q_A$ couple in PsbA1-PSII were found similar to those in plant PSII [23]. In contrast, in PsbA3-PSII the thermoluminescence of the $S_2Q_A^{\bullet-}$ charge recombination and the C≡N vibrational modes of bromoxynil detected in the reduced *minus* oxidized non-heme iron FTIR difference spectra supported either two binding sites or one binding site with two conformations [23].

In the present work, the effects of DCMU and bromoxynil binding have been studied by EPR and time-resolved UV–visible absorption spectroscopies in PsbA1-PSII and PsbA3-PSII from *T. elongatus*. It is shown that 1) the affinity of DCMU and bromoxynil for PSII in the $Q_A^{\bullet-}$ state strongly differs, consistent with the respective shifts undergone by the midpoint potential of $Q_A^{\bullet-}/Q_A$ in the presence of these inhibitors, and 2) the affinity of DCMU and bromoxynil for PSII in the $Q_AFe^{III}Q_B$ state differs in PsbA1-PSII and PsbA3-PSII which indicates a different midpoint potential of the non-heme iron in PsbA1-PSII and PsbA3-PSII. Moreover, the observation of a DCMU-induced oxidation of the non-heme iron strongly suggests that Fe^{III} is the Q_2 electron acceptor previously revealed by Joliot and Joliot [30,31].

2. Materials and methods

The biological material used was His-tagged PSII core complexes purified from 1) *T. elongatus* WT* cells, a strain in which both the $psbA_1$ and $psbA_2$ genes have been deleted and which therefore only expresses $psbA_3$ [32], 2) 43H cells [33] which express the $psbA_1$ gene [23,34] and 3) the D2-Y160F cells [35] which are expected to also express the $psbA_1$ gene. PSII purification was done as previously described [23,32].

Absorption changes were measured with a lab-built spectrophotometer [36] where the absorption changes are sampled at discrete times by short flashes. These flashes were provided by a neodymium: yttrium–aluminum garnet (Nd:YAG, 355 nm) pumped optical parametric oscillator, which produces monochromatic flashes (1 nm full-width at half-maximum) with a duration of 5 ns. Excitation was provided by a dye laser (685 nm, 10–15 mJ) pumped by the second harmonic of a Nd:YAG laser. The path length of the cuvette was 2.5 mm. PSII was used at 25 μg of Chl ml^{-1} in 10% glycerol, 1 M betaine, 15 mM $CaCl_2$, 15 mM $MgCl_2$, and 40 mM MES (pH 6.5). PSII were dark-adapted for ≈1 h at room temperature (20–22 °C) before the addition of either 0.1 mM phenyl-*p*-benzoquinone (PPBQ, dissolved in ethanol) or 0.1 mM DCMU or 0.1 mM bromoxynil (dissolved in ethanol).

Cw-EPR spectra were recorded using a standard ER 4102 (Bruker) X-band resonator with a Bruker Elexsys 500 X-band spectrometer equipped with an Oxford Instruments cryostat (ESR 900). Flash illumination at room temperature was provided by a Nd:YAG laser (532 nm, 550 mJ, 8 ns Spectra Physics GCR-230-10). PSII samples at 1.1 mg of Chl ml^{-1} were loaded in the dark into quartz EPR tubes and further dark-adapted for 1 h at room temperature before being frozen in the dark to 198 K in a dry-ice ethanol bath and then transferred to and stored in liquid N_2. Prior to the measurements, the samples were transferred in the dark at 198 K in a dry-ice ethanol bath and degassed as already described [37]. The addition of PPBQ (0.5 mM, final concentration), DCMU and bromoxynil, dissolved in ethanol 95% was done in the dark. For the experiments reported in Figs. 1 and 2, the additions were done after the recording of the dark spectra. For the experiments reported in Figs. 3 to 9, the additions were done after the dark-adaptation. The DCMU and bromoxynil concentrations in stock solutions were adjusted so that the final ethanol concentration was ≤3% in all the conditions studied.

3. Results

Fig. 1 illustrates in detail the protocol used in this study. The spectra were recorded in PsbA3-PSII at 4.2 K in the absence (a, black spectrum) and presence (b, red spectrum) of PPBQ (Fig. 1A), of DCMU (Fig. 1B) and of bromoxynil (Fig. 1C). Spectra c (in blue) are the difference spectra spectrum b-*minus*-spectrum a in each corresponding panel.

In addition to the spectroscopic features sensitive to the addition of quinone analogues or herbicides which will be described below, the spectrum of the dark-adapted samples shows the following features: *i*) the g_z and g_y resonances of $Cytc_{550}$ and to a less extent of $Cytb_{559}$ at ≈2230 G and ≈2920 G, respectively [38–40], which are strongly saturated owing to the temperature and the microwave power conditions used here, *ii*) a signal at g = 4.3 (≈1600 G) and at g values ≥5 (between 500 and 1500 G) from contaminants Fe^{III} (which should

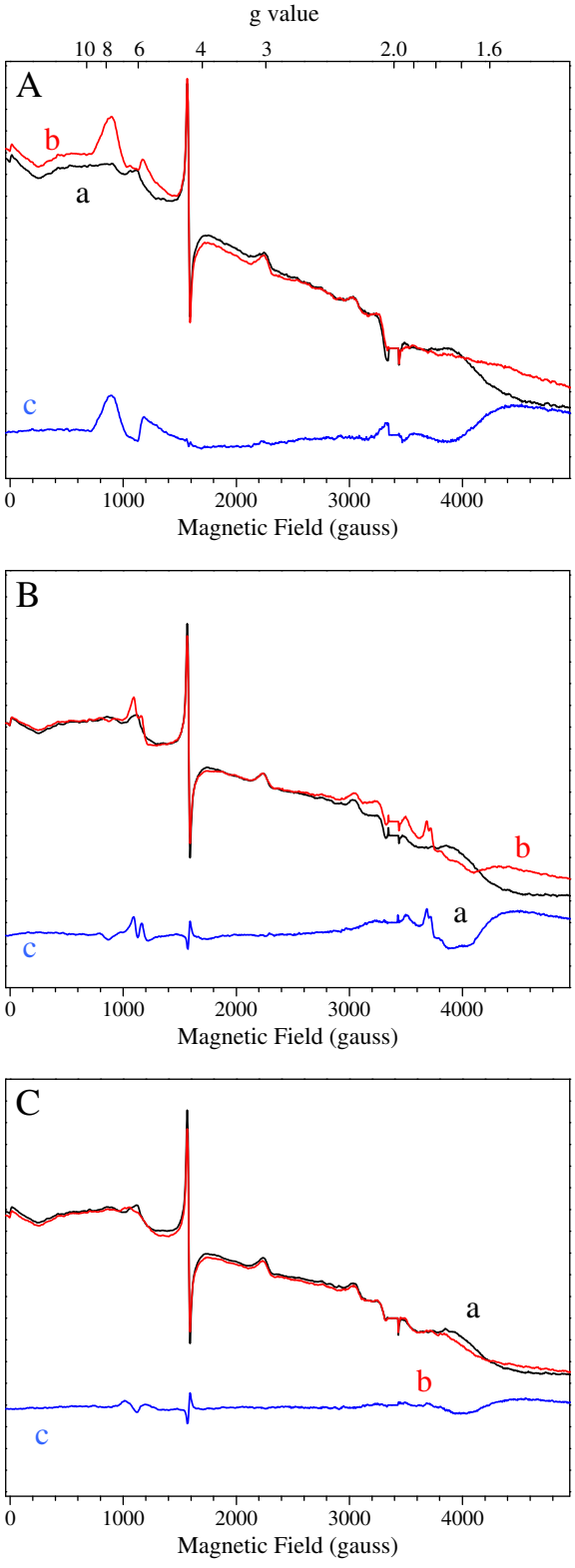

Fig. 1. EPR spectra recorded in PsbA3-PSII at 4.2 K. Effect of the addition of PPBQ (panel A), of DCMU (panel B), and of bromoxynil (panel C). Spectra a (black spectra) were recorded in dark-adapted PSII, spectra b (red spectra) were recorded after the addition of either PPBQ or DCMU or bromoxynil and spectra c (blue spectra) are the difference spectra after-*minus*-before the addition. Other instrument settings: [Chl] = 1.1 mg ml^{-1}; modulation amplitude, 25 G; microwave power, 20 mW; microwave frequency, 9.4 GHz; and modulation frequency, 100 kHz. The $Tyr_D^{\bullet}$ spectral region at g ≈ 2 was deleted.

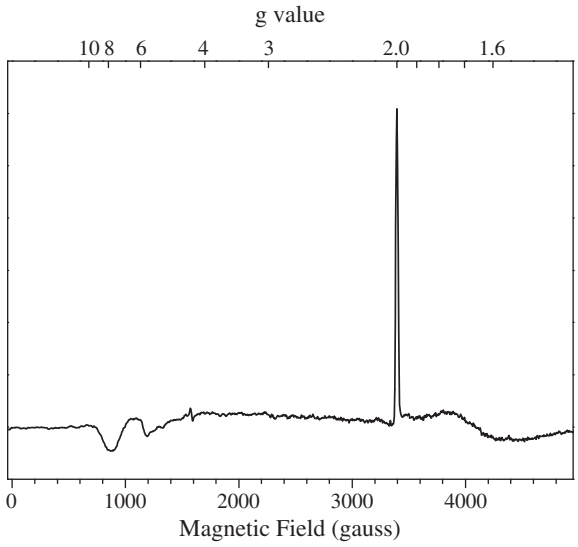

Fig. 2. EPR spectra recorded in D2-Y160F PSII at 4.2 K. The spectrum shown is the difference spectrum before-*minus*-after the addition of PPBQ. The same other instrument settings as in Fig. 1.

not be mistaken with the non-heme iron signal studied below), and *iii*) an out-off-scale narrow signal at g ≈ 2.0 (≈3400 G) from the $Tyr_D^{\bullet}$ which is deleted in the spectra shown. None of these signals were affected by the addition of the PPBQ or the herbicides.

The addition of PPBQ (Fig. 1A) resulted in the disappearance of the signal assigned to $Fe^{II}Q_B^{\bullet-}$, as shown by the negative $Fe^{II}Q_B^{\bullet-}$ signal in spectrum *c* between ≈3200 G and ≈4500 G, indicating that the dark-adapted PsbA3-PSII contained a significant amount of $Q_B^{\bullet-}$. The addition of PPBQ also induced the appearance of the non-heme Fe^{III} signal mainly detected by the two characteristic spectral features at g = 5.65 (≈1200 G) and g = 7.5 (≈900 G). As discussed in [41–43], the oxidant of the non-heme Fe^{II} is the semiquinone $PPBQ^{\bullet-}$ formed upon the reduction of PPBQ by $Q_B^{\bullet-}$: $Fe^{II} + PPBQ^{\bullet-} + 2H^+ \rightarrow Fe^{III} + PPBQH_2$.

The addition of DCMU (Fig. 1B) also resulted in the disappearance of the signal assigned to $Q_B^{\bullet-}$. In addition, it induced the appearance of several features (at 3700–4000 G, see spectrum *c*) which reflect the formation of $Q_A^{\bullet-}$ at the expense of $Q_B^{\bullet-}$ in agreement with the finding that DCMU shifts to the right hand term the following equilibria: $Q_AFe^{II}Q_B^{\bullet-} + DCMU \leftrightarrow Q_A^{\bullet-}Fe^{II}Q_B + DCMU \leftrightarrow Q_A^{\bullet-}Fe^{II}DCMU + Q_B$ [17,44], see also case (2) in Chart 1. The difference spectrum in the spectral range of the non-heme Fe^{III} includes a derivative shaped signal which reflects the well-known DCMU-induced changes of the zero-field splitting parameter of the S = 5/2 state of the non-heme Fe^{III} [43]. As such, this signal shows that the non-heme iron is oxidized in a low proportion of dark-adapted PsbA3-PSII even in the absence of any addition.

Although one would expect that the addition of bromoxynil (Fig. 1C) induces as well a modification of non-heme Fe^{III} signal, these changes were smaller than those observed upon the addition of DCMU (compare spectra in Fig. 1C and B) and this will be addressed below. The spectral changes detected in the quinone region between ≈3200 G and ≈4500 G upon the addition of bromoxynil are of smaller amplitude than the DCMU-induced ones. Moreover, we observed that the addition of ethanol alone resulted in similar spectral changes (not shown) so that we assign the spectral changes in Fig. 1C in the 3200–4500 G region to a solvent effect rather than to a displacement of the $Q_AFe^{II}Q_B^{\bullet-}$ + bromoxynil ↔ $Q_A^{\bullet-}Fe^{II}Q_B$ + bromoxynil ↔ $Q_A^{\bullet-}Fe^{II}$bromoxynil + Q_B equilibria. Consistent with this, bromoxynil addition induced no significant spectroscopic changes attributable to the formation of $Q_A^{\bullet-}$ suggesting that bromoxynil does not bind to PsbA3-PSII in which the $Q_B^{\bullet-}$ state is present.

The out-of-scale signal from the $TyrD^{\bullet}$ radical overlaps with the signal arising from the $Fe^{II}Q_B^{\bullet-}$ and thus precludes its full characterization. We

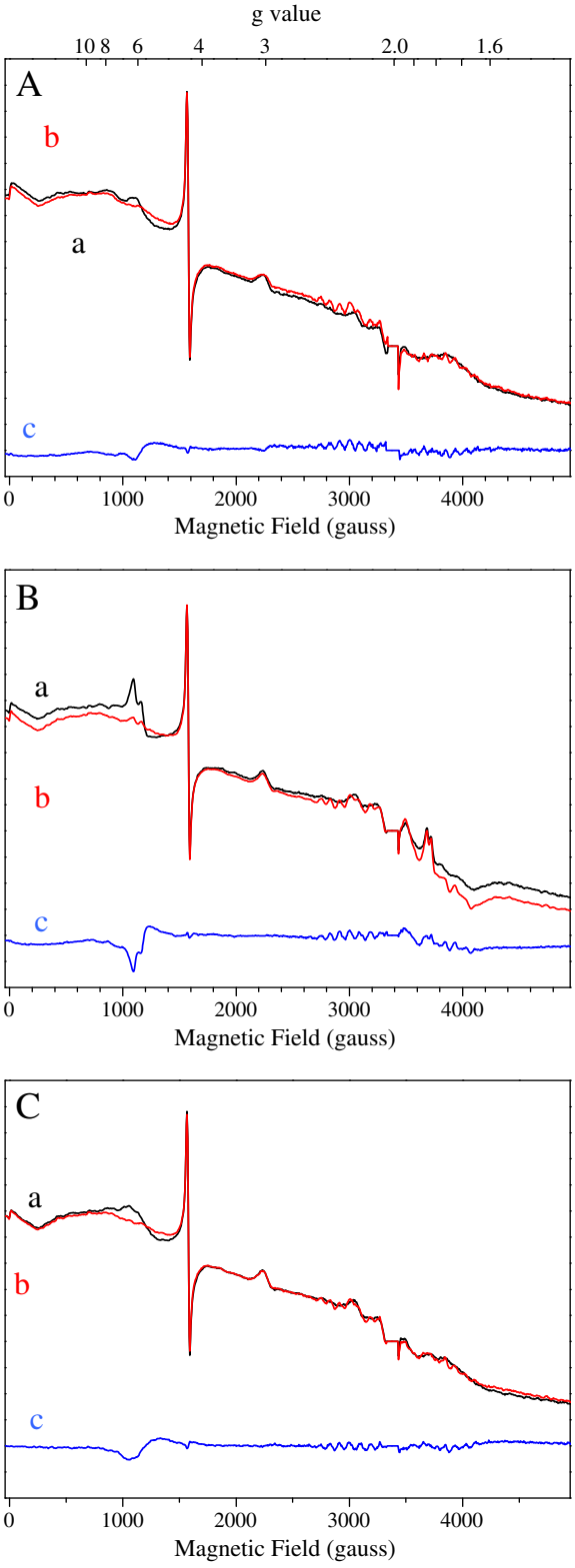

Fig. 3. EPR spectra recorded in PsbA3-PSII at 4.2 K. Spectra were recorded in the presence of 3% ethanol (panel A), in the presence of DCMU (panel B), and in the presence of bromoxynil (panel C). Spectra were recorded in dark-adapted samples (a, black spectra) and after one flash given at room temperature (b, red spectra). Spectra c (blue spectra) are the difference spectra after-*minus*-before the addition. The same other instrument settings as in Fig. 1. The $Tyr_D^{\bullet}$ spectral region at g≈2 was deleted.

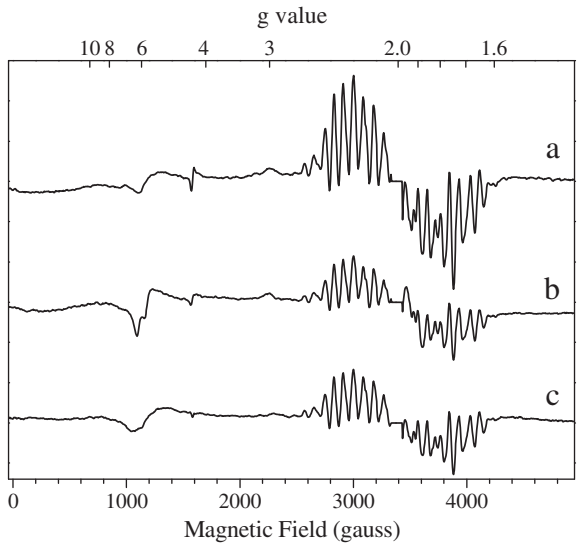

Fig. 4. EPR spectra recorded in PsbA3-PSII at 8.6 K. Spectra were first recorded in dark-adapted samples and then after one flash given at room temperature. The spectra shown are the light-*minus*-dark spectra in the presence of 3% ethanol (a), of DCMU (b), and of bromoxynil (c). The same other instrument settings as in Fig. 1. The $Tyr_D^{\bullet}$ spectral region at g≈2 was deleted.

thus repeated the same experiment (Fig. 2) as the one shown in Fig. 1A with the D2-Y160F mutant [35]. In these conditions, the difference spectrum before-*minus*-after the addition of PPBQ (spectrum *c*) exhibits the complete $Fe^{II}Q_B^{\bullet-}$ EPR signal which is detectable from ≈3000 to ≈5000 G. This signal will be described with more details by Sedoud et al. (manuscript submitted).

At this stage two major conclusions can be drawn: *i*) a significant fraction of PsbA3-PSII is in the $Q_B^{\bullet-}$ state in the dark, *ii*) whereas DCMU binding induces the formation of $Q_A^{\bullet-}$ at the expense of $Q_B^{\bullet-}$, bromoxynil does not at least up to a concentration of 200 μM. These conclusions may be further validated by measuring the flash-induced changes in the redox state of the various electron carriers in the PSII acceptor side, as illustrated in Fig. 3 which shows the flash-induced EPR spectra in the presence of ethanol (the solvent used here) (Fig. 3A) or DCMU (Fig. 3B) or bromoxynil (Fig. 3C). After addition of these chemicals, the spectra were recorded at 4.2 K prior to (spectra a) and after (spectra b) the illumination by 1 flash at room temperature. Spectra c are the difference spectra after-*minus*-before the flash illumination. Although the flash illumination should also induce the formation of the S_2-state, this one is strongly saturated, owing to the temperature and the microwave power conditions used here, which prevents an accurate estimation of its amplitude in these conditions.

In the presence of ethanol (Fig. 3A), we hardly detected any spectral changes between 3200 and 4500 G upon the flash illumination other than the strongly saturated S_2 multiline signal. This suggests that the proportion of the centers in the $Fe^{II}Q_B^{\bullet-}$ state was not modified by the flash illumination, or that, in other words, there was approximately 50% of PsbA3-PSII with $Fe^{II}Q_B^{\bullet-}$ in the dark-adapted state. The lack of $Q_A^{\bullet-}Fe^{II}$ formation in the absence of any artificial electron acceptor is in agreement with previous estimates in which at least 2 or 3 Q_B molecules are present per reaction center in PSII from *T. elongatus* [3,45–47]. We noted above that a fraction of PSII centers are in the non-heme Fe^{III} state, even in the absence of any addition. Expectedly, the light-induced charge separation leads to the reduction of the non-heme Fe^{III} as witnessed by the negative non-heme Fe^{III} signal with negative features at g = 5.65 (≈1200 G) and g = 7.5 (≈900 G) in spectrum *c* in Fig. 3A.

The results in Fig. 3B show that after the addition of DCMU the flash illumination induced the formation of a signal with a feature at g≈1.9 (≈3500 G) which is characteristic of $Q_A^{\bullet-}Fe^{II}$. The semiquinone radical is magnetically coupled to the high spin (S = 2) non-heme

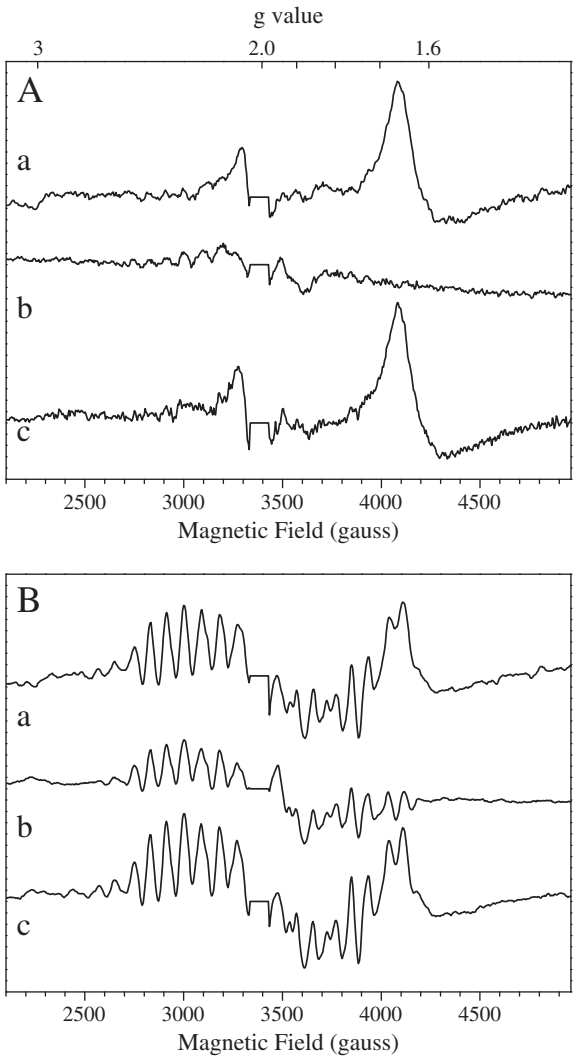

Fig. 5. EPR spectra recorded in PsbA3-PSII at 4.2 K (panel A) and at 8.6 K (panel B). Spectra were recorded in the presence of 3% ethanol (spectra a), in the presence of DCMU (spectra b), and in the presence of bromoxynil (spectra c). Spectra were recorded in dark-adapted samples and after a 198 K illumination. The spectra shown are the light-induced spectra. The same other instrument settings as in Fig. 1. The $Tyr_D^{\bullet}$ spectral region at $g \approx 2$ was deleted.

ferrous ion which is located between Q_A and Q_B [1–3] which gives rise to the broad EPR signals with turning points around $g \approx 1.8$ and 1.9, *e.g.* [45] and references therein. In principle, this signal can serve as a marker of the fraction of PSII centers with an oxidized Q_B before the addition of DCMU, since DCMU binding induces the formation of $Q_A^{\bullet-}Fe^{II}$ in the dark in those centers in the $Q_B^{\bullet-}$ state before addition. Yet, the picture may be slightly more complicated than that. Indeed, spectrum *c* in Fig. 3B shows that the negative signal in the non-heme Fe^{III} region was larger in the presence of DCMU than in its absence. This indicates that the fraction of centers in the non-heme Fe^{III} state in the dark is larger when DCMU is bound or that, in other terms, in addition to the $Q_AFe^{II}Q_B^{\bullet-} + DCMU \leftrightarrow Q_A^{\bullet-}Fe^{II}Q_B + DCMU \leftrightarrow Q_A^{\bullet-}Fe^{II}DCMU + Q_B$ equilibria, the following equilibria $Q_AFe^{II}Q_B^{\bullet-} + DCMU \leftrightarrow Q_AFe^{III}Q_BH_2 + DCMU \leftrightarrow Q_AFe^{III}DCMU + Q_BH_2$ might occur in PsbA3-PSII.

The results in Fig. 3C show that, in the presence of bromoxynil, the flash-induced signal assigned to $Q_A^{\bullet-}Fe^{II}$ was smaller than in the presence of DCMU. Moreover, in contrast to the DCMU case, the negative signal in the non-heme Fe^{III} region was similar in the presence of bromoxynil than in its absence. This indicates that bromoxynil binding does not affect the redox state of the non-heme iron. Thus, at variance with DCMU, bromoxynil does not shift the equilibria

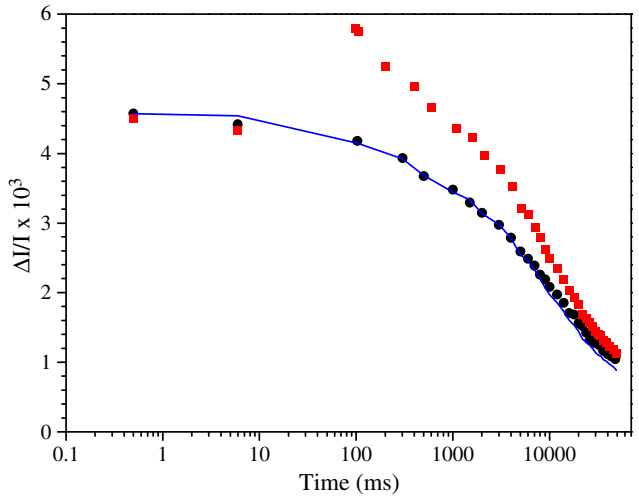

Fig. 6. Kinetics of the absorption changes at 320 nm in PsbA3-PSII. Black circles were recorded after the first saturating flash. For the red circles, measurements were done 500 μs and 6 ms after the first flash then a second saturating flash was given 100 ms after the first one. The continuous blue line is the decay after the second flash normalized to the same time scale and the same amplitude as that of the first flash. The samples (Chl = 25 μg ml^{-1}) were dark-adapted for 1 h at room temperature before the addition of 100 μM DCMU.

$Q_AFe^{II}Q_B^{\bullet-}$ + herbicide ↔ $Q_AFe^{III}Q_BH_2$ + herbicide ↔ Q_AFe^{III}herbicide + Q_BH_2 to the right, suggesting that bromoxynil has a lower affinity than DCMU for the centers in the Q_AFe^{III} state. All the results above and below are summarized in Chart 2.

All the spectra shown above were recorded at 4.2 K, a temperature which allows the detection of the non-heme iron signal and that of the quinone-Fe^{II} signals with almost no overlapping from the S_2 multiline signal. Yet, the S_2 multiline signal, being extremely specific of the advancement of the S-state cycle, is a reliable way to quantify the fraction of PSII centers in which a charge separation has occurred. By doing so, one can quantify the fraction of PSII centers in the $Q_A^{\bullet-}$ state prior to the flash and assess this quantity in the presence of either

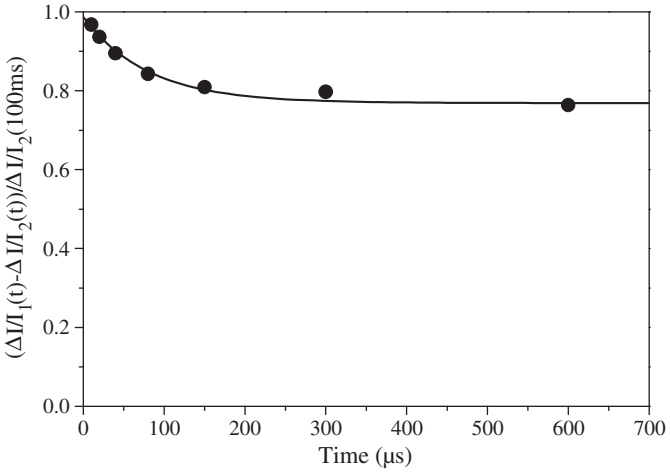

Fig. 7. Kinetics of the absorption changes at 552 nm in PsbA3-PSII after the first saturating flash of a sequence. The Y-axis is the difference between the amplitude of the ΔI/I measured at the indicated time after the first and second flases divided by the amplitude of the ΔI/I measured 100 ms after the second flash. The samples (Chl = 25 μg ml^{-1}) were dark-adapted for 1 h at room temperature before the addition of 100 μM DCMU. The fit was done with an exponential decay with an offset with OriginPro software (OriginLab Corporation).

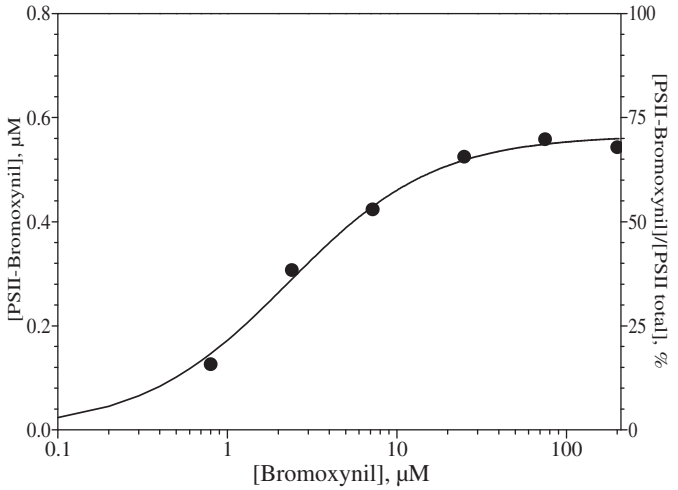

Fig. 8. [PSII-bromoxynil] *versus* the total bromoxynil concentration (black symbols). The [PSII-bromoxynil] concentration was estimated by measuring the absorption changes at 552 nm after a saturating flash at 10 μs and 10 ms and then by applying the following relation: [PSII-bromoxynil] = $(\Delta I/I^{10\ \mu s}{}_{+\text{bromox}} - \Delta I/I^{10\ ms}{}_{+\text{bromox}})/(\Delta I/I^{10\ \mu s}{}_{+\text{bromox}})$. The samples (Chl = 25 μg ml^{-1} = 0.8 μM) were dark-adapted for 1 h at room temperature before the addition of bromoxynil at the indicated concentrations. The fitting procedure was done with OriginPro software assuming a single binding site with the dissociation constant $K_d = [\text{PS II}]_{free}[I]_{free}/[\text{PSII-I}]$ with I for bromoxynil. After the straightforward substitutions we have: $Kd^*[\text{PSII-I}] = ([\text{PSII}]_{total}{}^*[I]_{total}) - ([\text{PSII}]_{total}{}^*[\text{PSII-I}]) - ([I]_{total}{}^*[\text{PSII-I}]) + [\text{PSII-I}]^2$.

DCMU or bromoxynil. We thus recorded the spectra at 8.6 K, with a microwave power of 20 mW, to detect the S_2 multiline signal in *T. elongatus* PSII. This signal is centered at g = 2 with at least 18 lines spaced by ≈90 G from ≈2500 to ≈4500 G and arises from an electronic spin S = 1/2 ground state in magnetic interaction with the nuclear spin I = 5/2 of the 4 Mn ions [48–50].

Fig. 4 shows the light-*minus*-dark spectra recorded in PsbA3-PSII at 8.6 K after a flash illumination in the presence of ethanol (spectrum a), in the presence of DCMU (spectrum b) or bromoxynil (spectrum c). As for the spectra measured at 4.2 K, the spectra measured at 8.6 K show that the non-heme Fe^{III} signal which disappeared upon the flash illumination

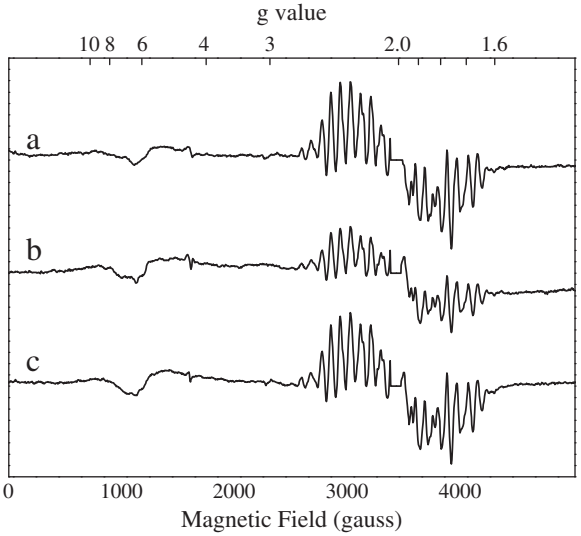

Fig. 9. EPR spectra recorded in PsbA1-PSII at 8.6 K. Spectra were first recorded in dark-adapted samples and then after one flash given at room temperature. The spectra shown are the light-*minus*-dark spectra in the presence of 3% ethanol (a), of DCMU (b), and of bromoxynil (c). The same other instrument settings as in Fig. 1. The $Tyr_D^{\bullet}$ spectral region at g≈2 was deleted.

had similar amplitude in the presence of bromoxynil and ethanol but a larger one in the presence of DCMU. The flash-induced S_2-multiline signal in the presence of DCMU and bromoxynil was approximately half that in the presence of ethanol alone. This is straightforwardly explained in the DCMU case since ≈50% of the PsbA3-PSII centers are in the closed $Q_A^{\bullet-}Fe^{II}$DCMU state before the flash illumination. In the bromoxynil case, we have shown above that the fate of the centers in the $Q_AFe^{II}Q_B^{\bullet-}$ case (which we estimated to be ≈50%) differs. Indeed, Fig. 1C showed that bromoxynil addition does not result in the formation of the $Q_A^{\bullet-}Fe^{II}$ state at the expense of $Q_AFe^{II}Q_B^{\bullet-}$ and that the relative amount of the latter stays unchanged. Thus one would expect to observe the formation of the S_2-state in the majority of the centers, if not all. However, we also noted earlier, that the relative amount of $Q_A^{\bullet-}Fe^{II}$ formed by the flash illumination (Fig. 3) is smaller in the presence of bromoxynil than in the presence of DCMU, suggesting that, under the conditions of the experiment, charge recombination occurs and leads to a decrease of the detectable amount of $S_2Q_A^{\bullet-}$ state. In a recent work, we have shown that the charge recombination between S_2 and $Q_A^{\bullet-}Fe^{II}$ in the presence of bromoxynil at room temperature occurs in the second time range in PsbA3-PSII [23]. The dark time between the flash illumination and the freezing of the sample (≈1–2 s) is thus long enough to allow the occurrence of the $S_2Q_A^{\bullet-}Fe^{II}$ charge recombination in a significant proportion of the centers. The data shown below shows that such is indeed the case.

Fig. 5 shows the light-*minus*-dark spectra recorded in PsbA3-PSII at 4.2 K (panel A) and at 8.6 K (panel B) after a 198 K illumination in the presence of either ethanol (spectra a), or DCMU (spectra b) or bromoxynil (spectra c). For reason of clarity, the spectral range shown from 2500 to 5000 G is focused on that including the S_2-multiline signal and the semiquinone signals.

The spectra recorded at 4.2 K (panel A) will be described in first. In the presence of ethanol only (spectrum a), the light-induced signal exhibited a large feature centered at g≈1.6 (≈4200 G) which is characteristic of the $Q_A^{\bullet-}Fe^{II}Q_B^{\bullet-}$ state *e.g.* [45,51]. This signal was formed in the centers with the $Q_AFe^{II}Q_B^{\bullet-}$ state present before the 198 K illumination since the electron transfer from Q_A to Q_B is blocked at such a temperature. The $Q_A^{\bullet-}Fe^{II}Q_B$ state, which is expected to be formed in the other centers, is also detected at g≈1.9 (3500–3600 G) *e.g.* [45,51,52]. Nevertheless the small amplitude of the $Q_A^{\bullet-}Fe^{II}$ signal in these EPR conditions together with the overlapping of the $Q_A^{\bullet-}Fe^{II}Q_B^{\bullet-}$ signal which is intrinsically much more intense makes the detection of the $Q_A^{\bullet-}Fe^{II}$ signal difficult. In the presence of DCMU (spectrum b) only the formation $Q_A^{\bullet-}Fe^{II}$ signal at g≈1.9 was detected (with the main feature between 3500 and 3700 G), showing that there were no remaining centers in the $Q_AFe^{II}Q_B^{\bullet-}$ prior to the 198 K illumination. In the presence of bromoxynil (spectrum c) the light-induced g = 1.6 signal from $Q_A^{\bullet-}Fe^{II}Q_B^{\bullet-}$ had a similar amplitude to that recorded in the absence of the herbicide (spectrum a). This again shows that in the centers with the $Q_AFe^{II}Q_B^{\bullet-}$ state before the addition of bromoxynil, the addition of this herbicide did not result in the formation of the $Q_A^{\bullet-}Fe^{II}$ bromoxynil state. The $Q_A^{\bullet-}Fe^{II}$ signal in spectrum c arises from centers in the $Q_AFe^{II}Q_B$ state prior to the 198 K illumination.

Panel B in Fig. 5 shows the difference spectra induced by the 198 K illumination and recorded at 8.6 K. In the absence of herbicide (spectrum a) the S_2-multiline signal is now fully detected in addition to the $Q_A^{\bullet-}Fe^{II}Q_B^{\bullet-}$ signal. In the presence of DCMU (spectrum b) the amplitude of the S_2-multiline signal was approximately half of that in spectrum a consistent with the estimate above that ≈50% of the centers were in the $Q_A^{\bullet-}Fe^{II}$DCMU state before the 198 K illumination. In the presence of bromoxynil (spectrum c), the amplitudes of both the $Q_A^{\bullet-}Fe^{II}Q_B^{\bullet-}$ signal and the S_2-multiline signal were similar to those observed in the absence of the herbicide, showing that the smaller amplitude of the S_2-multiline signal in the experiment after illumination by one flash and shown in Fig. 3 was due to a fast $S_2Q_A^{\bullet-}$ charge recombination which is prevented in the 198 K illumination procedure.

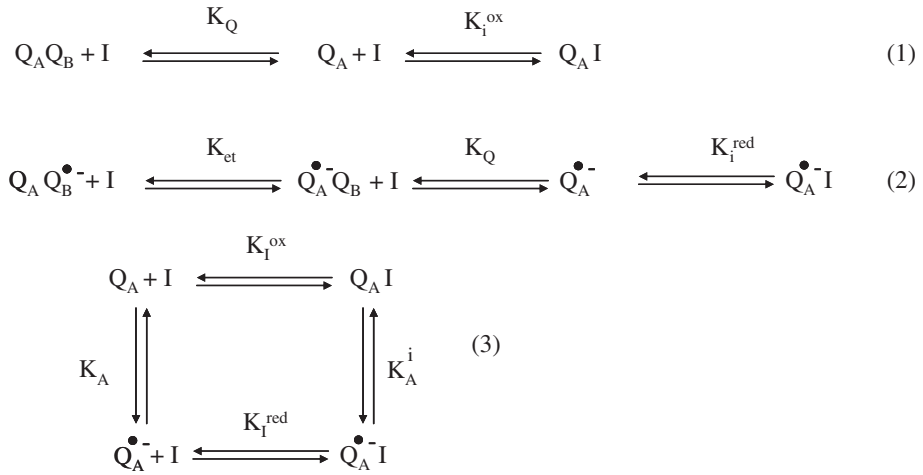

Chart 1. Thermodynamic equilibria describing the cases 1, 2 and 3 discussed in the text.

We have shown above that the non-heme iron, which is a potential electron acceptor in the Fe^{III} state, is oxidized in a small proportion of PsbA3-PSII and that this proportion increases in the presence of DCMU. This effect of DCMU was further investigated in the experiment reported in Fig. 6.

In Fig. 6, the absorption change in PsbA3-PSII was followed after the first and second saturating flashes given after the addition of DCMU to the dark-adapted sample. The measurement was done at 320 nm a wavelength which corresponds to a maximum in the $Q_A^{\bullet-}$-*minus*-Q_A difference spectrum and at which the S_2-*minus*-S_1 difference spectrum also contributes *e.g.* [53–57]. The filled black circles show the decay of the light-induced absorption change after the first flash. The first point was measured 500 μs after the flash. The red filled circles show the absorption changes measured 500 μs and 6 ms after a first flash and then the decay was followed after the second flash. The continuous blue line is the decay recorded after the second flash (red points) but with a time scale and amplitude scale rescaled to that recorded after the first flash. The kinetics of the decay after the second flash was similar to that after the first flash. The $S_2Q_A^{\bullet-}$ charge recombination in the presence of either DCMU or bromoxynil was recently studied in detail in both PsbA3-PSII and PsbA1-PSII [23]. Therefore, for the present purpose we will focus mainly on the amplitudes and less on the kinetics. The main difference between the black and red traces is the amplitude of the signal which is larger after the second flash than after the first flash. In the context of the model proposed above (see Chart 2) the results in Fig. 6 suggest that $Q_A^{\bullet-}$ is formed in all the centers after the first flash and reoxidized in less than 500 μs by the non-heme iron in the fraction of the centers in the Fe^{III} state prior to the flash illumination. In plant PSII, the half-time of this kinetics was measured to be ≈25 μs [42] but is unknown in *T. elongatus* samples. Therefore, this kinetics was measured in our sample and the result is shown in Fig. 7.

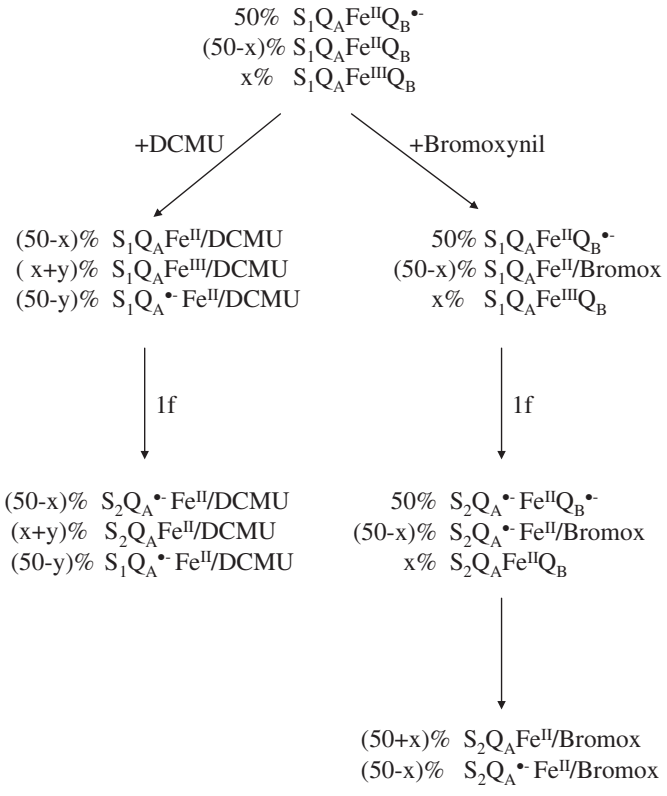

Chart 2. Schematic events following the first flash given on a dark-adapted PSII in the presence of either DCMU or bromoxynil. Centers in the S_0 state are not considered but they likely behave like those in the S_1 state.

In Fig. 7, $Q_A^{\bullet-}$ formation and reoxidation was followed at 552 nm in PsbA3-PSII as in [42]. This wavelength corresponds to the trough of the pheophytin band shift observed upon Q_A reduction [58–60] and is almost free from other spectral contributions, which is not the case at 320 nm [53–57]. The amplitude measured 10 μs after the flash of the signal was similar to that measured after the second one (not shown). This shows that $Q_A^{\bullet-}$ is indeed formed in all the centers after one saturating flash. Nevertheless, whereas the signal did not decay in the hundred μs time scale after the second flash, the signal decayed with a half-time close to 55 μs in ≈20% of the centers after the first flash, and we assign this decay to the $Q_A^{\bullet-}Fe^{III}DCMU \rightarrow Q_AFe^{II}DCMU$ reaction.

It is shown above that the binding of bromoxynil only occurred in centers in the Q_AQ_B state. To estimate the dissociation constant of bromoxynil for the Q_B pocket in PsbA3-PSII we have carried out the following experiment. The absorption changes were measured at 552 nm (as in Fig. 7, [42]) 10 μs and 10 ms after one flash. The amplitude at 10 μs corresponded to the maximum amount of $Q_A^{\bullet-}$ induced by one flash and was similar for all the bromoxynil concentrations used (not shown). From 10 μs to 10 ms the signal decayed in centers in which bromoxynil was not bound. This decay is due to the electron transfer from $Q_A^{\bullet-}$ to Q_B. The proportion of centers in which bromoxynil was bound was therefore estimated by the following relation: $[\text{PSII-bromoxynil}] = (\Delta I/I^{10\ \mu s}{}_{+\text{bromox}} - \Delta I/I^{10\ ms}{}_{+\text{bromox}})/(\Delta I/I^{10\ \mu s}{}_{+\text{bromox}})$. Fig. 8, filled circles, shows the [PSII-bromoxynil] concentrations as estimated above *versus* the total bromoxynil concentration together with a fit (continuous line) assuming one binding site. The PSII concentration was 25 μg Chl ml^{-1} which is equivalent to 0.8 μM. The

fitting procedure resulted in a dissociation constant equal to 2.3 μM and a binding of bromoxynil in ≈70% of the centers which suggests that in this experiment $Q_B^{\bullet-}$ was present in ≈30% of the centers.

All the results shown above were obtained in PsbA3-PSII. The results below now deal with PsbA1-PSII. In the experiment reported in Fig. 9, the PsbA1-PSII samples were illuminated by one flash at room temperature in the presence of either ethanol (spectrum a) or DCMU (spectrum b) or bromoxynil (spectrum c). Spectra were recorded at 8.6 K. It is noteworthy that the $S_2Q_A^{\bullet-}$ bromoxynil charge recombination is slower in PsbA1-PSII than in PsbA3-PSII [23] so that, as shown below, it was unnecessary to decrease the temperature at which the samples were illuminated to avoid charge recombination. The amplitudes of the S_2-multiline signal induced by one flash given at room temperature with and without bromoxynil were similar whereas the S_2-multiline signal was approximately half in the presence of DCMU. This shows that as for PsbA3-PSII, bromoxynil is unable to bind in centers in the $Q_A^{\bullet-}Fe^{II}$ state in PsbA1-PSII. This is further supported by the similar amplitude of the $Fe^{II}Q_B^{\bullet-}$ EPR signal in PsbA1-PSII before and after the addition of bromoxynil (not shown). Comparison of the amplitude of the S_2-multiline signal in the presence of DCMU with that in the two other conditions indicates that $Fe^{II}Q_B^{\bullet-}$ was also present in ≈50% of dark-adapted PsbA1-PSII.

Fig. 9 also shows that the amplitude of the non-heme Fe^{III} EPR signal which disappears upon flash illumination is similar in the 3 samples. This indicates that 1) as in PsbA3-PSII, there is a proportion of centers with an oxidized non-heme iron in the dark-adapted state in the absence of any addition but 2) in contrast to PsbA3-PSII, the addition of DCMU to PsbA1-PSII did not induce a further increase in the proportion of non-heme Fe^{III}. All the results obtained in the PsbA1-PSII were also obtained in the D2-Y160F sample (not shown) which is expected to express the *psbA1* gene under our growth conditions since it was constructed in a strain with the 3 *psbA* genes.

4. Discussion

The binding of a competitive inhibitor to the plastoquinone Q_B pocket requires the latter to be, at least transiently, empty [17,44]. On the basis of these premises, Lavergne and Velthuys distinguished two different cases depending on the redox state of Q_B in the dark. When Q_B is oxidized (case (1) in Chart 1), the respective binding probabilities of a plastoquinone and of the inhibitor will be determined by the competition between these two, *i.e.* by their respective affinity for the site and their concentration. The presence of Q_B in its semiquinone state (case (2) in Chart 1) does not prevent the binding of the inhibitor since the neutral state Q_B can be formed via the equilibrium between $Q_AQ_B^{\bullet-}$ and $Q_A^{\bullet-}Q_B$, yet it is expected to decrease the apparent affinity of the inhibitor for its site owing to the uphill character of this equilibrium. The addition of an inhibitor of the Q_B pocket is expected to displace the equilibrium between $Q_AQ_B^{\bullet-}$ and $Q_A^{\bullet-}Q_B$ in favor of the latter and hence to induce the formation of $Q_A^{\bullet-}$. These different expectations are satisfyingly met in the case of DCMU in plant PSII [44].

As discussed in [17,44] and documented in the Supplementary materials, the apparent dissociation constant of the inhibitor, which takes into account the competition of the occupancy of the Q_B pocket between plastoquinone and the inhibitor, is expected to depend on the redox state of Q_A. Importantly, this statement holds even when the intrinsic dissociation constants of the inhibitor, defined according to cases (1) and (2) as $K_i^{ox} = [Q_A][I]/[Q_AI]$ and $K_i^{red} = [Q_A^{\bullet-}][I]/[Q_A^{\bullet-}I]$, [I] being the free herbicide concentration, are equal, or in other terms when the binding constant of the inhibitor to the empty Q_B site does not depend on the redox state of Q_A one obtains: $K_{app}^{ox} = K_{app}^{red}/(1+K_{et})$ (see Supplementary material).

K_{et} has been estimated to be ≈20 [61], so that the dissociation constant/affinity constant of the inhibitor is expected to be about 20 fold larger/smaller when Q_A is in its semiquinone state. Whereas this is indeed the case for DCMU here, as in plant PSII [44], we found that, in the case of bromoxynil, the decrease in the apparent affinity constant for the $Q_A^{\bullet-}$ state is much larger than the above expectation. Indeed, the present results clearly indicate that in those centers in which $Q_B^{\bullet-}$ is present prior to the addition of the herbicide, the addition of DCMU results into the disappearance of the $Fe^{II}Q_B^{\bullet-}$ EPR signal and into the formation of the EPR signal characteristic of $Q_A^{\bullet-}Fe^{II}$. In contrast, upon the addition of bromoxynil, the $Fe^{II}Q_B^{\bullet-}$ EPR signal is not affected and no EPR signal from $Q_A^{\bullet-}Fe^{II}$ is detected. This indicates that an additional parameter participates to the modulation of the binding constant of bromoxynil by the redox state of Q_A. As we will now discuss, the bromoxynil-induced shift of the midpoint potential of the $Q_A^{\bullet-}/Q_A$ couple is a likely candidate. If one now neglects, temporarily and for the sake of simplicity, the competition between the inhibitor and the quinone binding and only consider the relationship between the redox state of Q_A and the binding properties of the inhibitor the Q_B pocket, one can describe the relevant equilibria as described in case (3) of Chart 1.

According to such a square diagram, the two midpoint potentials of the $Q_A^{\bullet-}/Q_A$ couple in the presence (E_m^i) and in the absence (E_m) of the herbicide are linked by the following relationship [62,63]:

$$E_m^i = E_m + \frac{RT}{nF}\ln\left(\frac{K_i^{red}}{K_i^{ox}}\right).$$

This relation shows that different affinities of the herbicide for the Q_A or $Q_A^{\bullet-}$ states respectively should translate into different midpoint potentials in the presence and absence of herbicides and *vice versa*. In addition, it shows that a larger (smaller) affinity for the semiquinone state than that for the oxidized state translates into an up-shift (down-shift) of the midpoint potential upon herbicide binding and *vice versa*. Krieger and colleagues have shown than DCMU and bromoxynil have opposite effect in this respect [28,29]. Whereas DCMU binding results in an up-shifted midpoint potential of the $Q_A^{\bullet-}/Q_A$ couple, bromoxynil binding induces a down-shift. Assuming at first that the amplitude of the down-shift is similar in *T. elongatus* PSII than in spinach PSII, the 45 mV down-shift would be equivalent to a ≈6 fold lower affinity of bromoxynil for the Q_B site in the $Q_A^{\bullet-}$ state than in the Q_A state. This, combined with the competition between quinone and bromoxynil binding, is expected to yield a ≈6* 20 = 120 fold smaller affinity for the semiquinone $Q_A^{\bullet-}$ state. We found here that the dissociation constant for bromoxynil is ≈2.3 μM when Q_A is oxidized. Thus, assuming a similar shift in the midpoint potential as the one observed in spinach PSII, the apparent dissociation constant when Q_A is in the semiquinone state would be ≈280 μM. We note that with 200 μM bromoxynil we observed no detectable binding in the $Q_A^{\bullet-}$ state, so that the down-shift of the midpoint potential of the $Q_A^{\bullet-}/Q_A$ couple upon the binding of bromoxynil is probably larger than 45 mV in *T. elongatus* PSII. It should be noted that a larger concentration range could not reliably be investigated owing to solubility problems and to secondary effects of bromoxynil on the Mn_4 cluster (mainly the appearance of some Mn^{2+}, not shown). Importantly, the above reasoning should also apply to DCMU binding. In other words, the reported up-shift of the midpoint potential of the $Q_A^{\bullet-}/Q_A$ couple observed upon DCMU addition is expected to translate into a larger affinity for DCMU when Q_A is in its semiquinone state. At odds with this expectation, the presence of $Q_B^{\bullet-}$ has been found to decrease the apparent binding constant of DCMU and, as discussed above, this decreased apparent binding constant has been rationalized by the competition between the binding of quinone and DCMU. An interesting possibility to account for the apparently contradictory findings that (*i*) DCMU binding up-shifts the midpoint potential of the $Q_A^{\bullet-}/Q_A$ couple (and thus stabilizes the semiquinone state) and (*ii*) DCMU binding to PSII in the $Q_A^{\bullet-}$ state is weaker, is that the binding constant of quinone to the Q_B pocket also depends on the redox state of Q_A. If indeed the binding constant of quinone also increases significantly in the presence of the $Q_A^{\bullet-}$, it may compensate the increased affinity for DCMU.

The above discussed finding that the binding constant of bromoxynil is strongly decreased in the presence of $Q_A^{\bullet-}$ raises the issue of the efficiency of this compound as an inhibitor of the Q_B pocket. Indeed, PSII centers in the Q_AQ_B state in the dark bind bromoxynil according to case (1) in Chart 1 with a rather low dissociation constant (≈2.3 μM, see above), but the flash-induced formation of the semiquinone $Q_A^{\bullet-}$ state may be expected to trigger the release of bromoxynil and hence open the gate for electron transfer. To our knowledge the binding and release rates of bromoxynil have not been determined. It is clear however that the release of bromoxynil is much slower than the charge recombination between S_2 and $Q_A^{\bullet-}$ since otherwise $Q_A^{\bullet-}$ would decay via forward electron transfer to Q_B rather than backward electron transfer to S_2. The fact that such is not the case is supported by several findings such as the down-shifted thermoluminescence glow curve observed in the presence of bromoxynil with respect to the DCMU case [23] or the concomitant decay of S_2 and $Q_A^{\bullet-}$ found when comparing kinetic data monitoring either one of the two partners, this work and [23]. The $S_2Q_A^{\bullet-}$ charge recombination rate in the presence of bromoxynil being ≈0.8 s^{-1} at 25 °C in the PsbA3 PSII [23], if we assume the dissociation constant to be larger than 250 μM (see above) the binding rate of bromoxynil (at 100 μM) would be smaller than 0.3 s^{-1} in the presence of $Q_A^{\bullet-}$. This figure is smaller than the one found for DCMU (≈5 s^{-1} at the same concentration [44]).

The present work is in agreement with a previous report which mentioned that the exchange of phenolic-type and urea-type herbicides in the Q_B site of spinach thylakoids occurred in the second time range [64] and that the exchange was faster for phenolic herbicides than for urea-type herbicides. It has also been found that in spinach thylakoids the dissociation constant of bromoxynil was larger in reducing conditions (K_d = 220 nM) than in oxidizing conditions (K_d = 45 nM) [65], despite a factor 10 in K_d values between these values and those reported here, which are difficult to rationalize differently than by invoking a species dependence.

In addition to the above conclusion that the binding constant of bromoxynil and DCMU is affected by the redox state of Q_A, the present results show that the addition of DCMU to centers in the $Q_AFe^{II}Q_B^{\bullet-}$ state induces the formation of the $Q_AFe^{III}Q_B$ state in a fraction of centers, this fraction being larger in PsbA3-PSII than in PsbA1-PSII (Fig. 3). This observation can also be explained in the framework of a square thermodynamic diagram such as the one depicted in case (3) in Chart 1 with the Fe^{II}/Fe^{III} redox couple in place of the $Q_A^{\bullet-}/Q_A$ couple. In this model, the midpoint potentials, E_m, of the Fe^{II}/Fe^{III} couple in the presence and in the absence of the herbicide are also expected to differ if indeed the binding constant of DCMU depends on the redox state of the non-heme iron. In support to this proposal, Wraight found that the redox state of the non-heme iron modulates the binding of DCMU [66].

The results in Figs. 3 and 4 also show that upon the addition of DCMU to a PsbA3-PSII sample, the herbicide-induced Fe^{III} EPR signal corresponds to a state in which the herbicide is bound whereas no extra Fe^{III} EPR signal was induced by the addition of bromoxynil. Therefore the same reasoning as above leads us to suggest that for the Fe^{II}/Fe^{III} couple: $E_m^{+\,DCMU} < E_m^{+\,bromox.}$ in PsbA3-PSII.

In contrast to PsbA3-PSII, the addition of either DCMU or bromoxynil to PsbA1-PSII did not result in an extra-oxidation of the non-heme iron. This suggests that the midpoint potential of the non-heme iron differs in PsbA3-PSII and PsbA1-PSII being probably more positive in PsbA1-PSII than in PsbA3-PSII at least when DCMU is bound. This is an additional difference between PsbA1-PSII and PsbA3-PSII with respect to those already pointed out [23].

From a structural standpoint, Q_A is connected to the Q_B binding pocket via a D2-His214-Fe-D1-His215 network through which the possible structural changes resulting from the occupation of the site can propagate to Q_A [1–3]. A recent FTIR study has shown that the frequency of the CO group of $Q_A^{\bullet-}$ is down-shifted in the presence of bromoxynil when compared to DCMU [67]. It is of note however that the IR bands corresponding to the C=O stretching modes of the neutral Q_A have, until now, remained elusive precluding the characterization of the likely differential effect of the bromoxynil, plastoquinone or DCMU on these modes. In any case, in the $Q_A^{\bullet-}$ state, the phenolate group of the phenolic herbicide forms a relatively strong H-bond with the NH group of D1-His215. Importantly, comparative docking calculations of bromoxynil, plastoquinone or DCMU suggest that the H-bond to this NH groups is stronger with bromoxynil than with PQ and with PQ than with DCMU [67]. Accordingly, these different occupants of the Q_B pocket are expected to differentially modify the Q_A–D2-His214–Fe–D1-His215 network and hence the midpoint potential of the $Q_A^{\bullet-}/Q_A$ couple. Moreover, the non-heme iron being part of this network it is also likely to undergo a shift of its midpoint potential, as proposed here, in response to the weakening of the strength of the H-bond in which the NH group of D1-His215 is involved, occurring when DCMU replaces plastoquinone.

The last point we would like to discuss is the observation that, by inducing the oxidation of the non-heme iron, addition of DCMU in the dark increases the number of potential electron acceptors on the first flash. This is reminiscent of the results which led Joliot and Joliot [30,31] to propose the existence of a second electron acceptor Q_2 in addition to Q_1, Q_1 being the other name of Q_A. The acceptor Q_2 has been shown to have no quinone properties. In the Q_1/Q_2 model, the existence of an oxidized Q_2 prior to the illumination prevented the full reduction of Q_1. From the results shown in this work, it seems likely that Fe^{III}, the concentration of which increasing upon the addition of DCMU in PsbA3-DCMU, corresponds to Q_2. In plant PSII, the half-time of the $Q_A^{\bullet-}Fe^{III}DCMU \rightarrow Q_AFe^{II}DCMU$ reaction was estimated to be 25 μs [42]. It was estimated here to be ≈55 μs in PsbA3-PSII in *T. elongatus*.

Acknowledgements

This study was supported by the JSPS and CNRS under the Japan-France Research Cooperative Program; Grant-in-Aid for Scientific Research from the Ministry of Education, Science, Sports, Culture and Technology (21612007 for M.S.); and in part by the EU/Energy Network project SOLAR-H2 (FP7 contract 212508). We would like to thank Jérôme Lavergne, Arezki Sedoud and Bill Rutherford for helpful discussions and for communicating results prior to publication. Thanh-lan Lai is acknowledged for technical assistance.

Appendix A. Supplementary data

Supplementary data to this article can be found online at doi:10.1016/j.bbabio.2010.10.004.

References

[1] K.N. Ferreira, T.M. Iverson, K. Maghlaoui, J. Barber, S. Iwata, Architecture of the photosynthetic oxygen-evolving center, Science 303 (2004) 1831–1838.
[2] B. Loll, J. Kern, W. Saenger, A. Zouni, J. Biesiadka, Towards complete cofactor arrangement in the 3.0 Å resolution structure of photosystem II, Nature 438 (2005) 1040–1044.
[3] A. Guskov, J. Kern, A. Gabdulkhakov, M. Broser, A. Zouni, W. Saenger, Cyanobacterial photosystem II at 2.9 Å resolution and the role of quinones, lipids, channels and chloride, Nat. Struct. Mol. Biol. 16 (2009) 334–342.
[4] J.W. Murray, K. Maghlaoui, J. Kargul, N. Ishida, T.-L. Lai, A.W. Rutherford, M. Sugiura, A. Boussac, J. Barber, X-ray crystallography identifies two chloride binding sites in the oxygen evolving centre of photosystem II, Energy Environ. Sci. 1 (2008) 161–166.
[5] K. Kawakami, Y. Umena, N. Kamiya, J.-R. Shen, Location of chloride and its possible functions in oxygen-evolving photosystem II revealed by X-ray crystallography, Proc. Natl. Acad. Sci. U. S. A. 106 (2009) 8567–8572.
[6] B.A. Diner, F. Rappaport, Structure, dynamics, and energetics of the primary photochemistry of photosystem II of oxygenic photosynthesis, Annu. Rev. Plant Biol. 53 (2002) 551–580.
[7] M.L. Groot, N.P. Pawlowicz, L.J. van Wilderen, J. Breton, I.H. van Stokkum, R. van Grondelle, Initial electron donor and acceptor in isolated photosystem II reaction centers identified with femtosecond mid-IR spectroscopy, Proc. Natl. Acad. Sci. U. S. A. 102 (2005) 13087–13092.

[8] A.R. Holzwarth, M.G. Muller, M. Reus, M. Nowaczyk, J. Sander, M. Rogner, Kinetics and mechanism of electron transfer in intact photosystem II and in the isolated reaction center: pheophytin is the primary electron acceptor, Proc. Natl. Acad. Sci. U. S. A. 103 (2006) 6895–6900.

[9] F. Rappaport, B.A. Diner, Primary photochemistry and energetics leading to the oxidation of the Mn_4Ca cluster and to the evolution of molecular oxygen in Photosystem II, Coord. Chem. Rev. 252 (2008) 259–272.

[10] G. Renger, T. Renger, Photosystem II: the machinery of photosynthetic water splitting, Photosynth. Res. 98 (2008) 53–80.

[11] H. Dau, I. Zaharieva, Principles, efficiency, and blueprint character of solar-energy conversion in photosynthetic water oxidation, Acc. Chem. Res. 42 (2009) 1861–1870.

[12] Y. Kato, M. Sugiura, A. Oda, T. Watanabe, Spectroelectrochemical determination of the redox potential of pheophytin a, the primary electron acceptor in photosystem II, Proc. Natl. Acad. Sci. U. S. A. 106 (2009) 17365–17370.

[13] A.R. Crofts, C.A. Wraight, The electrochemical domain of photosynthesis, Biochim. Biophys. Acta 726 (1983) 149–185.

[14] B. Bouges-Bocquet, Electron transfer between the two photosystems in spinach chloroplasts, Biochim. Biophys. Acta 14 (1973) 250–256.

[15] B.R. Velthuys, J. Amesz, Charge accumulation at the reducing side of system 2 of photosynthesis, Biochim. Biophys. Acta 333 (1974) 85–94.

[16] C.A. Wraight, Oxidation-reduction physical chemistry of the acceptor quinone complex in bacterial photosynthetic reaction centers: evidence for a new model of herbicide activity, Isr. J. Chem. 21 (1981) 348–354.

[17] B.R. Velthuys, Electron-dependent competition between plastoquinone and inhibitors for binding to photosystem II, FEBS Lett. 126 (1981) 277–281.

[18] B. Kok, B. Forbush, M. McGloin, Cooperation of charges in photosynthetic O_2 evolution. I. A linear four step mechanism, Photochem. Photobiol. 11 (1970) 457–475.

[19] P. Joliot, B. Kok. Oxygen evolution in photosynthesis; in: Bioenergetics of Photosynthesis (Govindjee, ed.), Academic Press, New York. 1975, pp. 387.

[20] Y. Nakamura, T. Kaneko, S. Sato, M. Ikeuchi, H. Katoh, S. Sasamoto, A. Watanabe, M. Iriguchi, K. Kawashima, T. Kimura, Y. Kishida, C. Kiyokawa, M. Kohara, M. Matsumoto, A. Matsuno, N. Nakazaki, S. Shimpo, M. Sugimoto, C. Takeuchi, M. Yamada, S. Tabata, Complete genome structure of the thermophilic cyanobacterium *Thermosynechococcus elongatus* BP-1, DNA Res. 9 (2002) 123–130.

[21] P.B. Kos, Z. Deak, O. Cheregi, I. Vass, Differential regulation of *psbA* and *psbD* gene expression, and the role of the different D1 protein copies in the cyanobacterium *Thermosynechococcus elongatus* BP-1, Biochim. Biophys. Acta 1777 (2008) 74–83.

[22] B. Loll, M. Broser, P.B. Kos, J. Kern, J. Biesiadka, I. Vass, W. Saenger, A. Zouni, Modeling of variant copies of subunit D1 in the structure of photosystem II from *Thermosynechococcus elongatus*, Biol. Chem. 389 (2008) 609–617.

[23] M. Sugiura, Y. Kato, R. Takahashi, H. Suzuki, T. Watanabe, T. Noguchi, F. Rappaport, A. Boussac, Energetics in photosystem II from *Thermosynechococcus elongatus* with a D1 protein encoded by either the *psbA1* or *psbA3* gene, Biochim. Biophys. Acta 1797 (2010) 1491–1499.

[24] S.A.P. Merry, P.J. Nixon, L.M.C. Barter, M.J. Schilstra, G. Porter, J. Barber, J.R. Durrant, D. Klug, Modulation of quantum yield of primary radical pair formation in photosystem II by site directed mutagenesis affecting radical cations and anions, Biochemistry 37 (1998) 17439–17447.

[25] F. Rappaport, M. Guergova-Kuras, P.J. Nixon, B.A. Diner, J. Lavergne, Kinetics and pathways of charge recombination in photosystem II, Biochemistry 41 (2002) 8518–8527.

[26] A. Cuni, L. Xiong, R.T. Sayre, F. Rappaport, J. Lavergne, Modification of the pheophytin midpoint potential in photosystem II: modulation of the quantum yield of charge separation and of charge recombination pathways, Phys. Chem. Chem. Phys. 6 (2004) 4825–4831.

[27] K. Cser, I. Vass, Radiative and non-radiative charge recombination pathways in photosystem II studied by thermoluminescence and chlorophyll fluorescence in the cyanobacterium *Synechocystis* 6803, Biochim. Biophys. Acta 1767 (2007) 233–243.

[28] A. Krieger-Liszkay, A.W. Rutherford, Influence of herbicide binding on the redox potential of the quinone acceptor in photosystem-II. Relevance to photodamage and phytotoxicity, Biochemistry 37 (1998) 17339–17344.

[29] A. Krieger-Liszkay, A.W. Rutherford, Herbicide-induced oxidative stress in photosystem II, Trends Biochem. Sci. 26 (2001) 648–653.

[30] P. Joliot, A. Joliot, Comparative-study of the fluorescence yield and of the C550 absorption change at room-temperature, Biochim. Biophys. Acta 546 (1979) 93–105.

[31] P. Joliot, A. Joliot, A photosystem-II electron-acceptor which is not a plastoquinone, FEBS Lett. 134 (1981) 155–158.

[32] M. Sugiura, A. Boussac, T. Noguchi, F. Rappaport, Influence of histidine-198 of the D1 subunit on the properties of the primary electron donor, P_{680}, of photosystem II in *Thermosynechococcus elongatus*, Biochim. Biophys. Acta 1777 (2008) 331–342.

[33] M. Sugiura, Y. Inoue, Highly purified thermo-stable oxygen-evolving photosystem II core complex from the thermophilic cyanobacterium *Synechococcus elongatus* having His-tagged CP43, Plant Cell Physiol. 40 (1999) 1219–1231.

[34] J.L. Hughes, N. Cox, A.W. Rutherford, E. Krausz, T.L. Lai, A. Boussac, M. Sugiura, D1 protein variants in photosystem II from *Thermosynechococcus elongatus* studied by low temperature optical spectroscopy, Biochim. Biophys. Acta 1797 (2010) 11–19.

[35] M. Sugiura, F. Rappaport, K. Brettel, T. Noguchi, A.W. Rutherford, A. Boussac, Site-directed mutagenesis of *Thermosynechococcus elongatus* photosystem II: the O_2 evolving enzyme lacking the redox active tyrosine D, Biochemistry 43 (2004) 13549–13563.

[36] D. Beal, F. Rappaport, P. Joliot, A new high-sensitivity 10-ns time-resolution spectrophotometric technique adapted to *in vivo* analysis of the photosynthetic apparatus, Rev. Sci. Instrum. 70 (1999) 202–207.

[37] S. Un, A. Boussac, M. Sugiura, Characterization of the tyrosine-Z radical and its environment in the spin-coupled $S_2Tyr_Z^\bullet$ state of Photosystem II from *Thermosynechococcus elongatus*, Biochemistry 46 (2007) 3138–3150.

[38] M. Roncel, A. Boussac, J.L. Zurita, H. Bottin, M. Sugiura, D. Kirilovsky, J.-M. Ortega, Redox properties of the photosystem II cytochromes b_{559} and c_{550} in the cyanobacterium *Thermosynechococcus elongatus*, J. Biol. Inorg. Chem. 8 (2003) 206–216.

[39] C.A. Kerfeld, M.R. Sawaya, H. Bottin, K.T. Tran, M. Sugiura, D. Cascio, A. Desbois, T.-O. Yeates, D. Kirilovsky, A. Boussac, Structural and EPR characterization of the soluble form of cytochrome *c*-550 and of the psbV2 gene product from the cyanobacterium *Thermosynechococcus elongatus*, Plant Cell Physiol. 44 (2003) 697–706.

[40] M. Sugiura, S. Harada, T. Manabe, H. Hayashi, Y. Kashino, A. Boussac, Psb30 contributes to structurally stabilise the photosystem II complex in the thermophilic cyanobacterium *Thermosynechococcus elongatus*, Biochim. Biophys. Acta 1797 (2010) 1546–1554.

[41] J.-L. Zimmermann, A.W. Rutherford, Photoreductant-induced oxidation of Fe^{2+} in the electron-acceptor complex of photosystem II, Biochim. Biophys. Acta 851 (1986) 416–423.

[42] V. Petrouleas, B.A. Diner, Light-induced oxidation of the acceptor-side Fe(II) of photosystem-II by exogenous quinones acting through the QB binding-site.1. Quinones, kinetics and pH-dependence, Biochim. Biophys. Acta 893 (1987) 126–137.

[43] B.A. Diner, V. Petrouleas, Light-induced oxidation of the acceptor-side Fe(II) of photosystem II by exogenous quinones acting through the QB binding site. 2. Blockage by inhibitors and their effects on the Fe(III) EPR spectra, Biochim. Biophys. Acta 893 (1987) 138–148.

[44] J. Lavergne, Mode of action of 3-(3, 4-dichlorophenyl)-1, 1-dimethylurea - evidence that the inhibitor competes with plastoquinone for binding to a common site on the acceptor side of Photosystem-II, Biochim. Biophys. Acta 682 (1982) 345–353.

[45] C. Fufezan, C.X. Zhang, A. Krieger-Liszkay, A.W. Rutherford, Secondary quinone in photosystem II of *Thermosynechococcus elongatus*: semiquinone-iron EPR signals and temperature dependence of electron transfer, Biochemistry 44 (2005) 12780–12789.

[46] J. Kern, B. Loll, C. Luneberg, D. DiFiore, J. Biesiadka, K.F. Irrgang, A. Zouni, Purification, characterisation and crystallisation of photosystem II from *Thermosynechococcus elongatus* cultivated in a new type of photobioreactor, Biochim. Biophys. Acta 1706 (2005) 147–157.

[47] R. Krivanek, J. Kern, A. Zouni, H. Dau, M. Haumann, Spare quinones in the Q_B cavity of crystallized photosystem II of *Thermosynechococcus elongatus*, Biochim. Biophys. Acta 1767 (2007) 520–527.

[48] J.M. Peloquin, R.D. Britt, EPR/ENDOR characterization of the physical and electronic structure of the OEC Mn cluster, Biochim. Biophys. Acta 1503 (2001) 96–111.

[49] M.-F. Charlot, A. Boussac, G. Blondin, Towards a spin coupling model for the Mn_4 cluster in photosystem II, Biochim. Biophys. Acta 1708 (2005) 120–132.

[50] L.V. Kulik, B. Epel, W. Lubitz, J. Messinger, Electronic structure of the Mn_4O_xCa cluster in the S_0 and S_2 states of the oxygen-evolving complex of photosystem II based on pulse Mn-55-ENDOR and EPR Spectroscopy, J. Am. Chem. Soc. 129 (2007) 13421–13435.

[51] A.R. Corrie, J.H.A. Nugent, M.C.W. Evans, Identification of EPR signals from the $Q_A^{\bullet-}Q_B^{\bullet-}$ and $Q_B^{\bullet-}$ in photosystem II from *Phormidium laminosum*, Biochim. Biophys. Acta 1057 (1991) 384–390.

[52] A.W. Rutherford, J.-L. Zimmermann, A new EPR signal attributed to the primary plastosemiquinone acceptor in photosystem II, Biochim. Biophys. Acta 767 (1984) 168–175.

[53] J.P. Dekker, H.J. vanGorkom, M. Brok, L. Ouwehand, Optical characterization of photosystem-II electron-donors, Biochim. Biophys. Acta 764 (1984) 301–309.

[54] G.H. Schatz, H.J. vanGorkom, Absorbency difference spectra upon charge-transfer to secondary donors and acceptors in photosystem-II, Biochim. Biophys. Acta 810 (1985) 283–294.

[55] J. Lavergne, Absorption changes of photosystem-II donors and acceptors in algal cells, FEBS Lett. 173 (1984) 9–14.

[56] J. Lavergne, Improved UV-visible spectra of the S-transitions in the photosynthetic oxygen-evolving system, Biochim. Biophys. Acta 1060 (1991) 175–188.

[57] G. Renger, B. Hansum, Studies on the deconvolution of flash-induced absorption changes into the difference spectra of individual redox steps within the water-oxidizing enzyme-system, Photosynth. Res. 16 (1988) 243–259.

[58] D.B. Knaff, D.I. Arnon, Spectral evidence for a new photoreactive component of oxygen-evolving system in photosynthesis, Proc. Natl. Acad. Sci. U. S. A. 63 (1969) 963–969.

[59] H.J. van Gorkom, Identification of reduced primary electron-acceptor of photosystem-II as a bound semiquinone anion, Biochim. Biophys. Acta 347 (1974) 439–442.

[60] D.H. Stewart, P.J. Nixon, B.A. Diner, G.W. Brudvig, Assignment of the Q$_y$ absorbance bands of photosystem II chromophores by low-temperature optical spectroscopy of wild-type and mutant reaction centres, Biochemistry 39 (2000) 14583–14594.

[61] B.A. Diner, Dependence of deactivation reactions of photosystem-II on redox state of plastoquinone pool-a varied under anaerobic conditions — equilibria on acceptor side of photosystem-II, Biochim. Biophys. Acta 460 (1977) 247–258.

[62] P.L. Dutton, D.F. Wilson, Redox potentiometry in mitochondrial and photosynthetic bioenergetics, Biochim. Biophys. Acta 346 (1974) 165–212.

[63] J. Alric, Y. Pierre, D. Picot, J. Lavergne, F. Rappaport, Spectral and redox characterization of the heme c(i) of the cytochrome *b*(6)*f* complex, Proc. Natl. Acad. Sci. U. S. A. 102 (2005) 15860–15865.

[64] W.F.J. Vermaas, G. Dohnt, G. Renger, Binding and release kinetics of inhibitors of Q_A^- oxidation in thylakoid membranes, Biochim. Biophys. Acta 765 (1984) 74–83.
[65] W.F.J. Vermaas, G. Renger, C. Arntzen, Herbicide/quinone binding interactions in photosystem II, Z. Naturforsch. 39c (1984) 368–373.
[66] C.A. Wraight, Modulation of herbicide-binding by the redox state of Q_{400}, an endogenous component of photosystem II, Biochim. Biophys. Acta 809 (1985) 320–330.
[67] R. Takahashi, K. Hasegawa, A. Takano, T. Noguchi, Structures and binding sites of phenolic herbicides in the QB pocket of photosystem II, Biochemistry 49 (2010) 5445–5454.